

See discussions, stats, and author profiles for this publication at: <https://www.researchgate.net/publication/259111797>

# Growth of High-Density-Aligned and Semiconducting-Enriched Single-Walled Carbon Nanotubes: Decoupling...

Article in ACS Nano · December 2013

DOI: 10.1021/nn405105y · Source: PubMed

CITATIONS

23

READS

85

8 authors, including:



Jinghua Li

Northwestern University

6 PUBLICATIONS 86 CITATIONS

[SEE PROFILE](#)



Shibo Liang

Peking University

13 PUBLICATIONS 187 CITATIONS

[SEE PROFILE](#)



Lian-Mao Peng

Peking University

461 PUBLICATIONS 11,798 CITATIONS

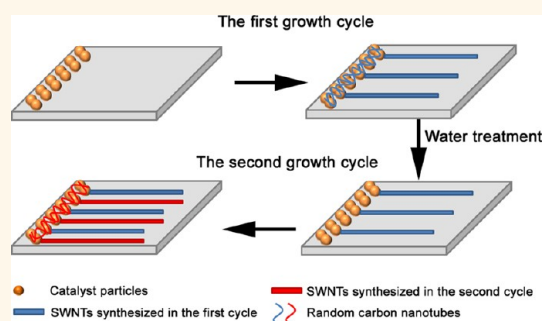
[SEE PROFILE](#)

# Growth of High-Density-Aligned and Semiconducting-Enriched Single-Walled Carbon Nanotubes: Decoupling the Conflict between Density and Selectivity

Jinghua Li,<sup>†</sup> Kaihui Liu,<sup>‡</sup> Shibo Liang,<sup>§</sup> Weiwei Zhou,<sup>†</sup> Matthieu Pierce,<sup>‡</sup> Feng Wang,<sup>‡</sup> Lianmao Peng,<sup>§</sup> and Jie Liu<sup>†,\*</sup>

<sup>†</sup>Department of Chemistry, Duke University, Durham, North Carolina 27708, United States, <sup>‡</sup>Department of Physics, University of California at Berkeley, Berkeley, California 94720, United States, and <sup>§</sup>Key Laboratory for the Physics and Chemistry of Nanodevices and Department of Electronics, Peking University, Beijing 100871, China

**ABSTRACT** Single-walled carbon nanotubes (SWNTs) are highly desired for future electronic applications due to the excellent electrical, mechanical, and thermal properties. However, the density and the selectivity in the growth of aligned semiconducting nanotubes do not coexist previously: when the selectivity is high, the density is low and *vice versa*. In the present work, we found that random carbon nanotubes (CNTs) in the catalyst area block the growth of aligned SWNTs along the lattice structure on the quartz surface, thus significantly reducing the density of nanotubes during growth. More interestingly, it was shown that the random CNTs can be selectively removed through appropriate treatments using water vapor as an *in situ* etchant while the aligned SWNTs survive even after long-time water vapor treatment. To obtain high-density semiconducting SWNT arrays, we designed an improved multiple-cycle growth method, which included the treatment of SWNTs with water vapor after each growth cycle without cooling the system. Using this method, we have successfully obtained dense semiconducting SWNTs ( $\sim 10$  SWNTs/ $\mu\text{m}$ ) over large areas and with high uniformity.



**KEYWORDS:** single-walled carbon nanotubes · multiple-cycle growth method · water vapor · high density · high selectivity

Single-walled carbon nanotubes (SWNTs) have attracted considerable attention in nanoelectronics because of their outstanding electrical and thermal properties.<sup>1–10</sup> Particularly, dense parallel SWNT arrays are found to have great potential for making radio frequency (RF) devices due to their considerable improvements in the on-driving current, mobility, and cutoff frequency.<sup>11–13</sup> More recently, researchers at IBM have demonstrated sub-10 nm transistors using carbon nanotubes for high-speed and power-efficient logic applications.<sup>14</sup> However, in order to realize such applications, high-density and high-purity semiconducting nanotubes are needed because (i) dense SWNT arrays can carry higher current and are more robust for

integrated circuits and (ii) high selectivity for semiconducting SWNTs is required to obtain high on/off ratios in SWNT-based field-effect transistors (FETs).<sup>5,14–20</sup> Currently, there are two competing approaches: one is to deposit preselected semiconducting nanotubes on the substrate, which has been recently demonstrated by the IBM group. The other is the directly controlled growth by chemical vapor deposition (CVD) method for horizontally aligned SWNT arrays.<sup>21–23</sup> The direct growth method is generally thought to provide nanotubes of better quality since the nanotubes do not need to go through purification, sonication, and separation procedures that are known to create defects on the nanotubes. However, the density and

\* Address correspondence to j.liu@duke.edu.

Received for review October 1, 2013 and accepted December 2, 2013.

Published online December 02, 2013  
10.1021/nn405105y

© 2013 American Chemical Society

selectivity of nanotubes from the direct growth methods are still far from ideal.

Over the past decade, great progress has been made in achieving the goals using the CVD method. On one hand, the density and alignment of SWNT arrays have been greatly improved.<sup>11,12</sup> For example, as reported in a recent work by our group, the density of SWNT arrays has been increased to 20–40 SWNTs/ $\mu\text{m}$  by using a multiple-cycle CVD growth method with ethanol/methanol as carbon feedstocks.<sup>13</sup> On the other hand, several groups have successfully synthesized predominantly semiconducting or metallic SWNTs.<sup>24–31</sup> Despite the great success in synthesizing aligned SWNT arrays, the goal of simultaneously obtaining high density and high selectivity has not been achieved until now. In general, it is believed that, within a certain range, the high-concentration carbon feedstock can increase the SWNT density.<sup>32</sup> However, it is also known that the high concentration of the carbon feeding source usually reduces the selectivity of SWNTs, as clearly indicated in the recent work published by our group.<sup>33</sup> In this sense, a lower carbon feeding rate is believed to be necessary for obtaining high-purity semiconducting SWNTs. Thus fabricating the aligned SWNT arrays with both high density and high selectivity is currently a challenge. It is highly desired to find a reliable method that decouples the asynchronous relationship between the density and selectivity of SWNTs.

In our current study, we observed an important fact that random carbon nanotubes (CNTs) in the area of the catalyst can block the growth of the aligned SWNTs along the lattice structure on the quartz surface. Such blocking is one of the main causes that reduced the total density of the aligned nanotubes and created nonuniformity in the SWNT arrays. More interestingly, it is found that an appropriate treatment using water as an *in situ* etchant can exclusively remove random CNTs, while most of the aligned SWNTs remain intact. Furthermore, an improved multiple-cycle CVD method is demonstrated which uses a low concentration of carbon feedstock and introduces water to the system to ensure the high selectivity of semiconducting SWNTs. The SWNTs were treated by water after each growth cycle to remove the random CNTs. After five growth cycles, the density of SWNT arrays can be as high as around 10 SWNTs/ $\mu\text{m}$  with significantly improved uniformity, which is 4–5 times higher than that of SWNTs produced by one-cycle growth method. Micro-Raman and single-tube optical spectroscopy measurements further confirm that the SWNTs made by this method are of high selectivity.

## RESULTS AND DISCUSSION

Our study is motivated by the observation that in the catalyst area there are some randomly aligned CNTs, which blocked the aligned SWNTs growing along the lattice structure on the quartz surface. Figure 1a shows

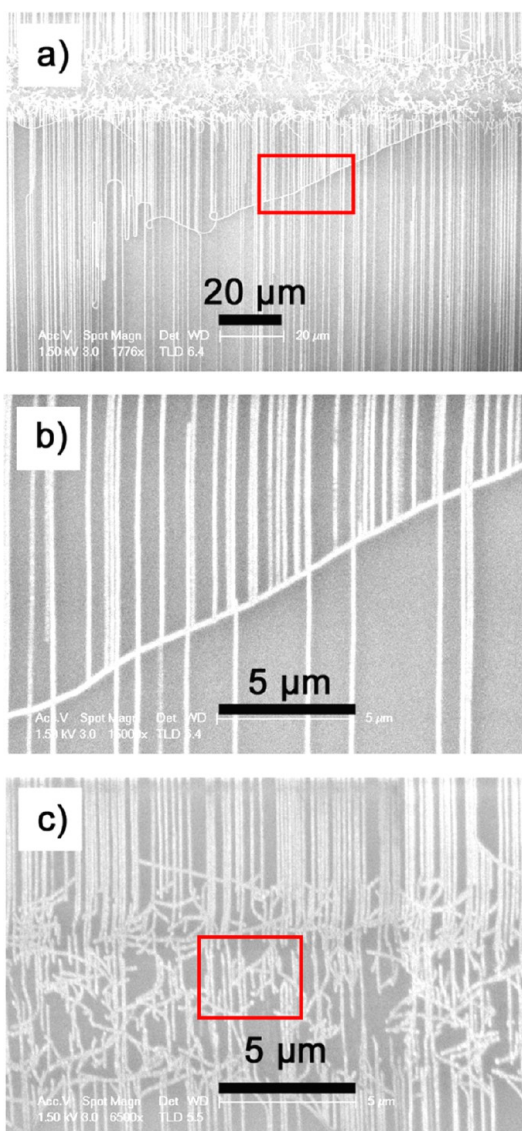


**Figure 1.** SEM images showing (a) the random CNTs that block the growth of aligned SWNTs, (b) the details in the location labeled by the red rectangle in panel (a), and (c) the aligned SWNTs blocked by the random CNTs in the region where catalysts are deposited.

a representative SEM image describing such a fact, and Figure 1b is the locally enlarged image. Similarly, the aligned SWNTs are also blocked by the random CNTs in the region where catalysts are deposited, as shown in the box in Figure 1c. From these SEM images, it is very clear that the growth of most aligned SWNTs terminates when they reach random CNTs in front and only a few of them can cross over. These observations demonstrated that the random CNTs caused a sharp decrease in the density of SWNTs and created nonuniformity in the sample. Therefore, the presence of random CNTs could be a crucial factor that prevents us from obtaining SWNT arrays with high density. In this sense, it is necessary to remove the random CNTs using an etchant in order to obtain dense SWNT arrays. A recent study published by us<sup>33</sup> showed that

water vapor can be used as an effective *in situ* etchant for the metallic nanotubes to selectively grow

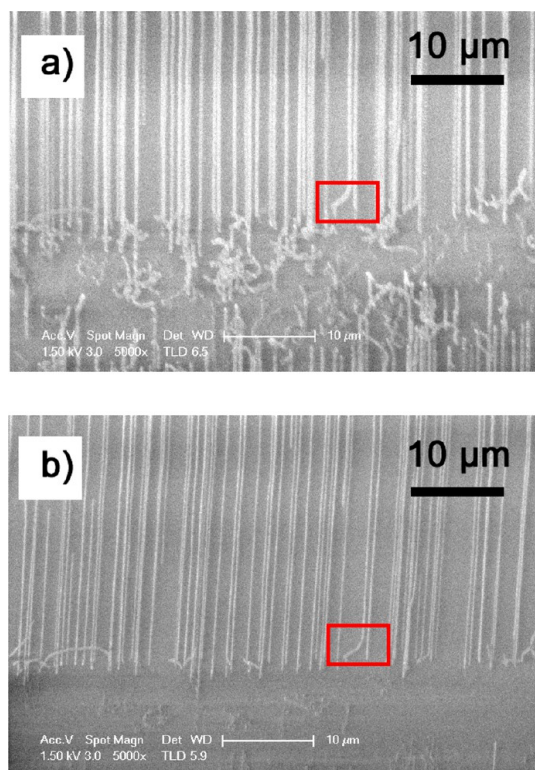


**Figure 2.** SEM images of a sample before (a) and after (b) water vapor treatment. The areas labeled by red rectangles are at the exact same location of the sample and are used as a marker.

semiconducting-enriched SWNT arrays on quartz substrates. In some experiments, we also observed the disappearance of nanotubes in the catalyst regions.<sup>13,33</sup> Is water vapor also capable of removing the random CNTs standing on the quartz lattice? To answer this question, a set of experiments has been carried out by varying both the water vapor concentration in the CVD chamber carrier and the etching time. Surprisingly, after being treated by water vapor at the concentration between 356 and 586 ppm for an appropriate time, the random CNTs in the catalyst area have been completely removed, while most of the aligned SWNTs remain intact even if such a treatment lasts for a long time. Figure 2 shows the SEM images of a sample before (panel a) and after (panel b) water vapor treatment, where the areas labeled by red rectangles are at exactly the same location on the sample and are used as position markers. Clearly, as shown by Figure 2b, the small misaligned CNTs in Figure 2a have been removed after water treatment.

The selective etching effect of water vapor for the random CNTs can be understood as follows. First, more catalyst particles around the random CNTs may accelerate the etching reaction.<sup>34,35</sup> This is supported by the observation that when the as-prepared arrays were treated by oxygen plasma, a much stronger etchant than water, most of the SWNTs were oxidized from the tips where the catalyst particles exist (see Figure S1 in the Supporting Information). In addition, the random CNTs consist of SWNTs and multiwalled nanotubes (MWNTs), the latter of which may have more defects

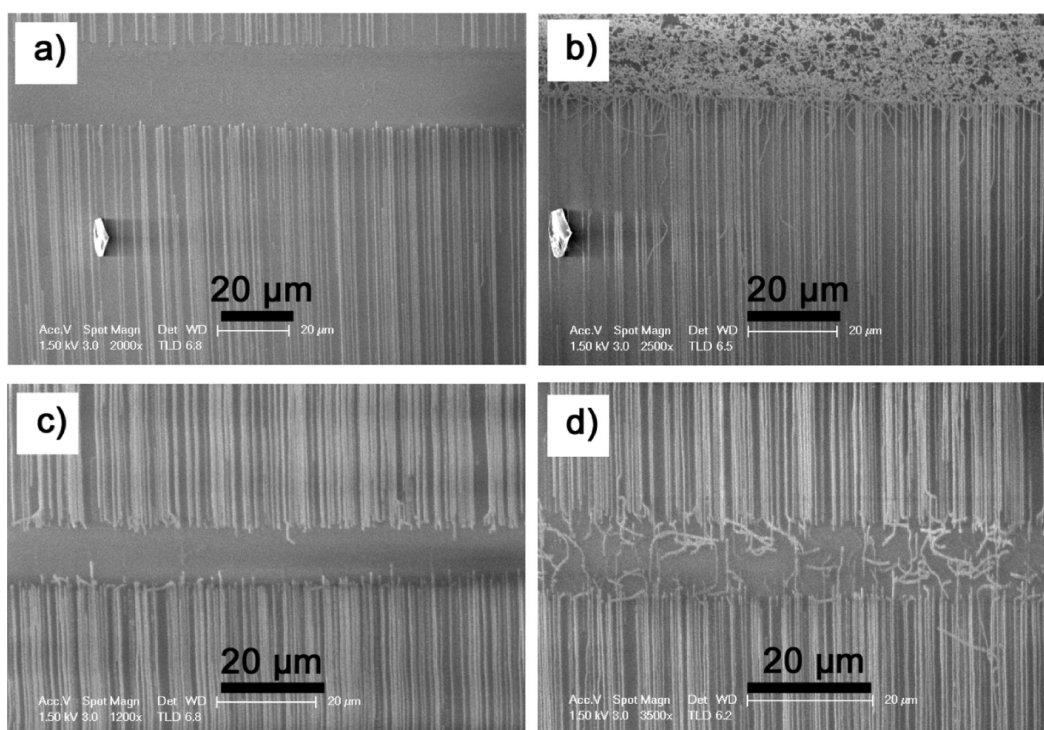


**Figure 3.** SEM images of two CNT samples before (a,c) and after (b,d) the second-time growth.

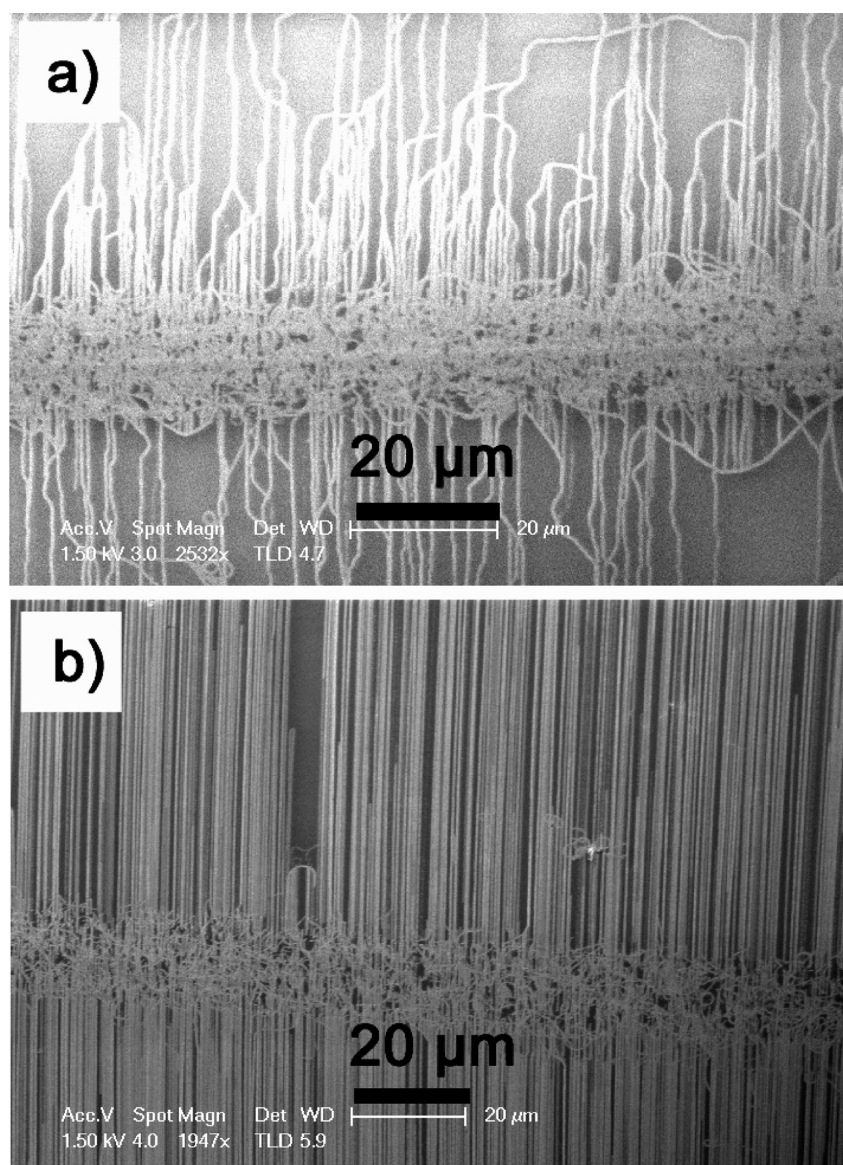


**Figure 4.** SEM images of misaligned CNTs on the wafer annealed after the second-time growth (a) and well-aligned CNTs on the same wafer nucleated by new catalysts after removing all the curved CNTs (b).

and hence could be easily attached by oxidants such as water. In contrast, the aligned SWNTs are more stable and cannot be etched by the oxidant (water) due to their structural integrity.

On the basis of the observations above, we designed a growth method which synthesizes SWNTs repetitively after removing the random CNTs in the catalyst area by treating them with water vapor, hoping to increase the density of aligned nanotubes. Figure 3 shows results before and after the second-time growth. There are some new SWNTs appearing after the new growth cycle, indicating that some catalyst particles still keep their activity after the first-time growth. However, as shown in Figure 3b,d, the newly grown SWNTs are not well-aligned. To better understand this observation, we annealed the sample in air at 900 °C until all the CNTs were removed. Then a new

cycle of growth was performed on the same substrate, and it is found that nearly all newly grown SWNTs are curved, as shown in Figure 4a. Considering the fact that the growth conditions were kept the same during our experiments, we came up with two possible explanations for the misalignment of the newly grown SWNTs: (i) the lattice structure of the quartz wafer could be destroyed, and (ii) the catalyst could have aggregated after the repetitive heating and cooling and the long-time treatment under high temperature.

To test which hypothesis is correct, the same sample was annealed in air at 900 °C to remove all the CNTs again. Then new catalysts were redeposited on the quartz wafer and another growth cycle was performed. As shown in Figure 4b, the newly synthesized SWNTs are well-aligned, which confirms the second hypothesis. This is consistent with previous results that the

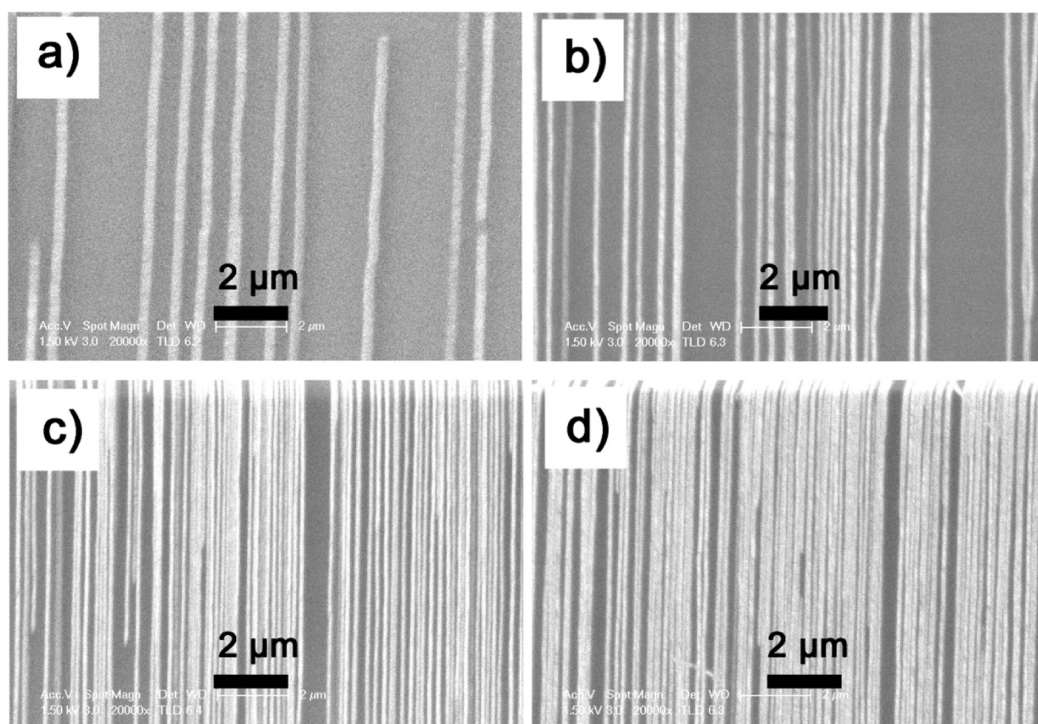


**Figure 5.** SEM images of horizontally aligned SWNTs on the quartz surface by one-cycle growth (a), two-cycle growth (b), four-cycle growth (c), and five-cycle growth (d) under the same CVD growth condition (Ar flow through ethanol bubbler at 90 sccm, another Ar flow through water bubbler at 30 sccm and H<sub>2</sub> flow at 279 sccm).

diameter distribution of SWNTs is closely related to the size of the catalyst particles.<sup>32</sup> The increase of the size of catalyst particles may lead to the larger diameters of SWNTs, and the alignment force tends to decrease as the diameters of SWNTs increase,<sup>11,36</sup> which may cause the SWNTs to become misaligned. In fact, the atomic force microscopy (AFM) result shows that the curved nanotubes have larger diameters than normal aligned SWNTs synthesized by one-cycle growth method (see Figure S2 in the Supporting Information).<sup>25,36,37</sup>

To limit the aggregation of the catalyst, one strategy is to avoid the repetitive heating and cooling procedures as well as the long-time treatment under high temperature. This can be achieved by combining all growth cycles and etching cycles in one process (see Methods for details). We refer to such a method as the improved multiple-cycle growth method to distinguish it from the multiple-cycle growth method discussed in our previous work.<sup>13</sup> Figure 5 shows the SEM images of horizontally aligned SWNT arrays after the one-, two-, four-, and five-cycle growth, respectively. From these results, it is clear that the density of SWNT arrays increased from 1–2 SWNTs/ $\mu\text{m}$  for the one-cycle growth (panel a) to 2–4 SWNTs/ $\mu\text{m}$  for the two-cycle growth (panel b) and 4–6 SWNTs/ $\mu\text{m}$  for the four-cycle growth (panel c), and finally reached around 10 SWNTs/ $\mu\text{m}$  (panel d). Figure S3 in the Supporting Information shows the diameter distributions for SWNT arrays prepared *via* the one-cycle, three-cycle, and five-cycle methods measured by AFM. It is observed that

the average diameters obtained from these three steps are 1.89, 1.97, and 2.01 nm, respectively, showing a slight upshift trend of the nanotube diameter. This is consistent with the theory of Ostwald ripening.<sup>38,39</sup> It should be noted that no further increase in the density of SWNT arrays was observed when more growth cycles were performed, which might be attributed to the deactivation of the catalyst particles under high temperature. Obviously, this improved multiple-cycle growth method significantly increased the density of SWNT arrays by using a low carbon feeding rate and introducing water into the system, which are necessary for obtaining the high-purity semiconducting SWNTs.

The other issue we are concerned about is the selectivity of as-prepared SWNTs. To answer this question, resonant Raman spectroscopy (RRS) was used to characterize the SWNT arrays prepared *via* the five-cycle growth method. It is well-known that RRS is an exceedingly powerful tool for characterizing SWNTs to reveal the electronic and phonon properties of SWNT arrays. The radial breathing mode (RBM) of the Raman spectrum assigns and distinguishes the semiconducting and metallic SWNTs. We used lasers with two different wavelengths of 633 and 785 nm and characterized 15 spots on the sample prepared *via* the five-cycle growth method. The measured results are shown in Figure 6, and the black and red rectangles marked with M and S correspond to frequency ranges where RBM peaks of metallic and semiconducting SWNTs are expected, respectively. The peaks at 128, 205, and

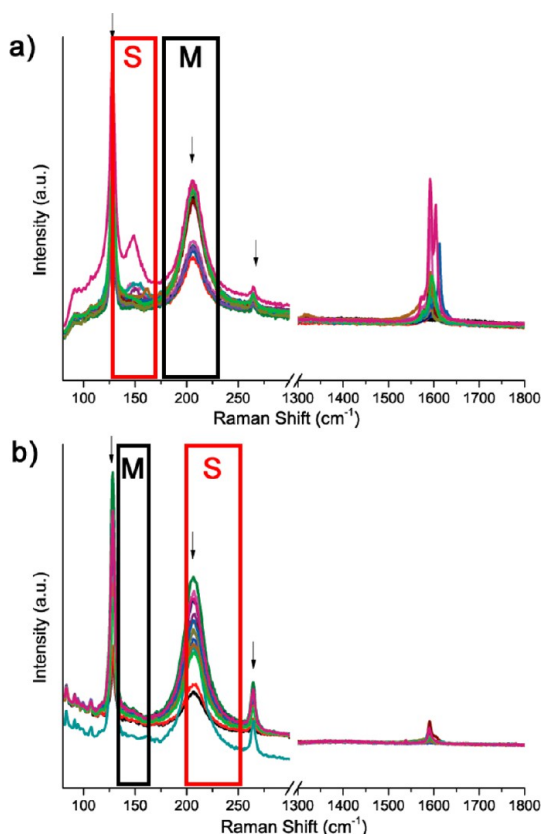


**Figure 6.** Raman spectra of the SWNT array prepared *via* the five-cycle growth. The spectra were collected from 15 different spots on the sample surface with excitation laser lines of 633 (a) and 785 (b) nm. The peaks at 128, 205, and 264  $\text{cm}^{-1}$  marked by the arrows are sourced from the quartz substrate. The black and red rectangles marked with M and S correspond to the frequency ranges where RBM peaks of metallic and semiconducting SWNTs are expected, respectively.

264  $\text{cm}^{-1}$  marked with black arrows are sourced from the quartz substrate.

When a 633 nm laser was used for excitation, as shown in Figure 6a, in the red rectangle, the frequency range where RBM peaks of semiconducting SWNTs are expected, we observed evident signals of semiconducting SWNTs and the distribution of the RBM frequencies is between 146 and 161  $\text{cm}^{-1}$ . From the experimental relationship between a SWNT diameter ( $d$ , in nm) and an RBM shift ( $\omega$ , in  $\text{cm}^{-1}$ ),  $\omega = 248/d$ ,<sup>40</sup> the diameters of these observed semiconducting tubes are estimated to be between 1.5 and 1.7 nm. In contrast, no other peaks but those from the quartz substrate at 205  $\text{cm}^{-1}$  are visible in the black rectangle that corresponds to the frequency range where RBM peaks of metallic tubes are expected. From the Raman data shown in Figure 6a, it is believed that the improved multiple-cycle growth method produces a large proportion of semiconducting SWNTs. When a 785 nm excitation laser was used, no RBM peaks of semiconducting tubes are visible (Figure 6b). This is because at 785 nm laser only the semiconducting tubes with a diameter smaller than 1.13 nm can show

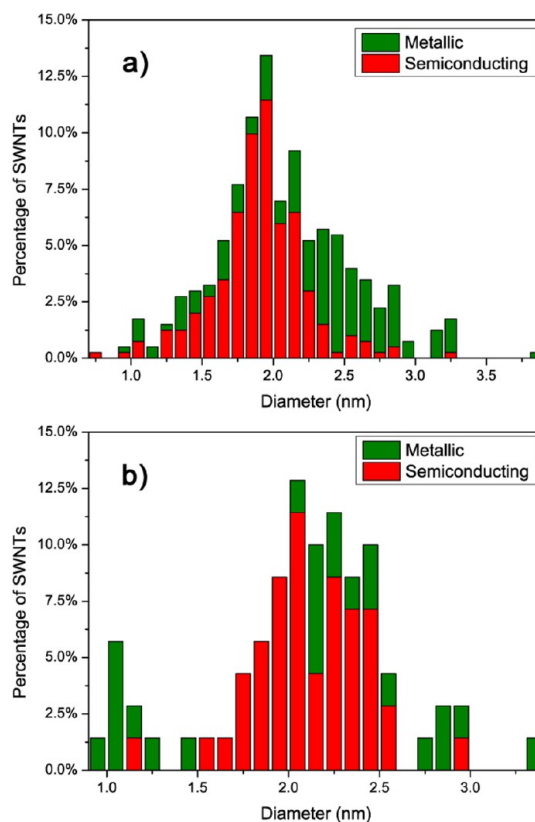


**Figure 7.** Diameter and chirality distribution of the SWNTs synthesized *via* one-time growth (15 min, panel a) and three-cycle growth (panel b) under the same growth condition mentioned in the Methods section measured by the optical imaging and spectroscopy.

RBM signals. On the other hand, in Figure 6b, there are also no observable RBM peaks of metallic tubes, indicating the presence of few metallic SWNTs within the diameter range from 1.5 to 1.9 nm. The current results confirm that the improved multiple-cycle CVD method predominantly synthesizes semiconducting SWNTs in the diameter range smaller than 2 nm. In addition, the disorder band (D-band) was barely observed in the Raman spectra, meaning that the water vapor treatment did not bring about significant defects of SWNTs.

To further investigate the selectivity of the as-prepared SWNT arrays, a detailed study on chirality distribution was performed on substrate by our newly developed polarization-based optical homodyne microscope/spectroscopy combined with a supercontinuum laser light source.<sup>41</sup> This technique was proven to be very powerful to identify the chiral index of individual nanotubes with high accuracy and efficiency. Figure 7a,b shows the distribution of semiconducting and metallic SWNTs within different diameter ranges *via* the one-time and three-cycle growth methods under the same growth condition which is described in the Methods section (Figure 7a was also used in one of our earlier publications<sup>41</sup>). Note that the density of SWNTs prepared by five-cycle growth is too high to provide an optical spectrum for assigning

the chirality of individual tubes. As shown in Figure 7, the ratios of the semiconducting SWNTs to the metallic counterparts (S/M ratios) are 1.48 and 1.92, respectively, and both of the values are much higher than that of the controlled group synthesized by the same recipe but without water (0.97; see Figure S4 in the Supporting Information). The result confirms that the improved multicycle growth method provides increased density and selectivity for semiconducting SWNTs simultaneously. Interestingly, it is shown that the S/M ratios are not equally distributed within different diameter ranges: for both the one-time and three-cycle growth methods, the semiconducting SWNTs are highly enriched in the diameter range of 1.5–2.2 nm and the S/M ratios are 4.68 and 5.20, while for the SWNTs synthesized without water, the value is only 1.26. Figure S5 in the Supporting Information shows the transport properties of top-gated FET based on SWNT arrays prepared by the five-cycle growth method. According to the observed chirality distribution, we proposed that not only the electronic structure of SWNTs but also the diameter and the concentration of water significantly influence the reactivity between SWNTs and water. For SWNTs of small diameter, local strain plays a more important role than the electronic structure since oxidation is preferential in areas of high curvature.<sup>42–44</sup> Consequently, all small-diameter SWNTs are sensitive to water, and no obvious selectivity can be found under some certain growth conditions. For SWNTs within the diameter range from 1.5 to 2.2 nm, the concentration of water optimized in this study could mainly etch the metallic SWNTs while the majority of semiconducting SWNTs can survive.

To support this hypothesis, one additional experiment was performed using the same growth condition mentioned in the Methods section with 50 min postsynthesis etching (water concentration: 506 ppm). The chirality distribution of as-prepared SWNTs was mapped out in Figure S6 in the Supporting Information. The diameter-dependent etching rule still applies even after postsynthesis etching for 50 min. This fact indicates that the water concentration and the property of SWNTs have a combined action on the selectivity. Though detailed study on the diameter-dependent selectivity is still needed, the current results shed light on the future research direction in further improving the selectivity for semiconducting SWNTs:

diameter control and selective etching should be combined.

For comparison, we also did Raman measurement on SWNTs made by the previous multiple-cycle growth method (see Figure S7 in the Supporting Information).<sup>13</sup> According to Figure S7, RBM signals are not found in either the metallic or the semiconducting regions. It is well-known that RBM signals of SWNTs with diameters larger than 2 nm are hardly detected by Raman spectroscopy. Thus the absence of RBM signals in Figure S7 is attributed to the large diameter of SWNTs synthesized using the previous multiple-cycle growth method.<sup>13</sup> That is also supported by the AFM result that shows the diameter distribution of SWNTs made in our previous work<sup>13</sup> is  $2.4 \pm 0.5$  nm. In contrast, the present improved multiple-cycle growth method can synthesize the SWNT arrays with relatively smaller diameters, as shown in Figure 7. The large-diameter-based field-effect transistors showed a low on/off ratio, indicating little, if any, selectivity for SWNT arrays made by the previous method. The uniqueness of the improved multiple-cycle growth method is that it synthesizes high-density and high-selectivity SWNT arrays with smaller diameters.

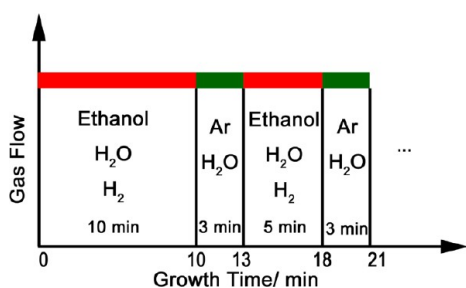
## CONCLUSIONS

In summary, the present work shows that (i) the random CNTs in the catalyst area are a crucial factor that prevents us from obtaining the high-density and high-quality semiconducting SWNTs, and (ii) the repetitive treatment of samples under high temperature can result in the aggregation and deactivation of the catalyst. More interestingly, we have found that the selective removal of random carbon nanotubes can be achieved by the treatment using an appropriate amount of water vapor. Most importantly, we have presented an improved multiple-cycle growth method to synthesize high-density, high-quality, and semiconducting-enriched SWNT arrays on quartz substrates. Using the improved multiple-cycle growth method, we have obtained the dense semiconducting-enriched SWNT arrays ( $\sim 10$  SWNTs/ $\mu\text{m}$ ) over large areas and with high uniformity. We have successfully decoupled the asynchronous relationship between the density and selectivity of SWNTs. Such understanding on the growth mechanism will be shown to be very useful for future nanoelectronics applications.

## METHODS

**Improved Multiple-Cycle Growth Method.**  $\text{CuCl}_2$ /poly(vinylpyrrolidone) alcohol solution was used as the precursor and patterned on Y-cut single-crystal quartz wafers for the SWNT growth.<sup>36</sup> The substrate with catalyst precursor deposited on it was then annealed for 30 min in the 1 in. Linderberg furnace in air at 775 °C to remove the polymers in the catalyst precursor and to form  $\text{Cu}_x\text{O}_y$ . After the samples cooled to room

temperature, the furnace was heated to and kept at 775 °C for 25 min in  $\text{H}_2$  atmosphere at  $\sim 367$  sccm to reduce  $\text{Cu}_x\text{O}_y$  nanoparticles to Cu nanoparticles. The CVD growth was then performed at 900 °C. In a typical growth experiment, an argon flow through an ethanol bubbler at  $\sim 90$  sccm, another argon flow through a water bubbler at 30 sccm, and a hydrogen flow at  $\sim 279$  sccm were introduced into the system in the first cycle of growth for 10 min. After the first growth cycle, the flow



**Scheme 1.** Experimental flow diagram for the synthesis of aligned SWNTs using the improved multiple-cycle growth method.

through the water bubbler was kept on and the rest of the flows were turned off. An argon flow at  $\sim 391$  sccm was introduced into the system to maintain the stable pressure in the chamber of the furnace. The etching process took 3 min. The next growth cycle was the same as the first one except that the growth time was 5 min instead of 10 min. The experimental flow diagram is shown in Scheme 1.

**Characterization.** A scanning electron microscope (SEM, FEI XL30 S-FEG, operated at 1.5 kV), an atomic force microscope (AFM, Digital Instruments Multiple Mode SPM Nanoscope IIIa, operated at tapping-mode), and a micro-Raman spectroscopy (Horiba Jobin Yvon LabRam ARAMIS) were used for the characterization of synthesized SWNTs. The optical imaging and spectroscopy for the chirality distribution of SWNTs were performed following a previously reported method.<sup>41</sup>

**Fabrication of FET Devices.** Top-gated FET devices with a channel length of  $2 \mu\text{m}$  and a width of  $100 \mu\text{m}$  were patterned by e-beam lithography. Pd (50 nm) was deposited by e-beam evaporation as the contact metal. The gate dielectric is  $\text{Y}_2\text{O}_3$  oxidized with 2.7 nm Y. Ti (20 nm) was used as the gate metal.

**Conflict of Interest:** The authors declare no competing financial interest.

**Acknowledgment.** This work is supported by a grant from NSF (CHE-1213469). The authors also acknowledge the support from Duke SMIF (Shared Materials Instrumentation Facilities).

**Supporting Information Available:** Additional SEM and AFM images, chirality distributions, electrical measurement, and Raman spectra. This material is available free of charge via the Internet at <http://pubs.acs.org>.

## REFERENCES AND NOTES

- Bockrath, M.; Cobden, D. H.; McEuen, P. L.; Chopra, N. G.; Zettl, A.; Thess, A.; Smalley, R. E. Single-Electron Transport in Ropes of Carbon Nanotubes. *Science* **1997**, *275*, 1922–1925.
- Chen, Z.; Appenzeller, J.; Lin, Y. M.; Sippel-Oakley, J.; Rinzler, A. G.; Tang, J.; Wind, S. J.; Solomon, P. M.; Avouris, P. An Integrated Logic Circuit Assembled on a Single Carbon Nanotube. *Science* **2006**, *311*, 1735.
- Dresselhaus, M. S.; Dresselhaus, G.; Eklund, P. C. In *Science of Fullerenes and Carbon Nanotubes: Their Properties and Applications*; Academic Press: San Diego, CA, 1996.
- Iijima, S.; Ichihashi, T. Single-Shell Carbon Nanotubes of 1-nm Diameter. *Nature* **1993**, *363*, 603–605.
- Javey, A.; Guo, J.; Wang, Q.; Lundstrom, M.; Dai, H. J. Ballistic Carbon Nanotube Field-Effect Transistors. *Nature* **2003**, *424*, 654–657.
- Javey, A.; Kim, H. S.; Brink, M.; Wang, Q.; Ural, A.; Guo, J.; McIntyre, P.; McEuen, P.; Lundstrom, M.; Dai, H. J. High- $\kappa$  Dielectrics for Advanced Carbon-Nanotube Transistors and Logic Gates. *Nat. Mater.* **2002**, *1*, 241–246.
- Pop, E.; Mann, D.; Wang, Q.; Goodson, K.; Dai, H. Thermal Conductance of an Individual Single-Wall Carbon Nanotube above Room Temperature. *Nano Lett.* **2006**, *6*, 96–100.

- Saito, R.; Dresselhaus, G.; Dresselhaus, M. S. In *Physical Properties of Carbon Nanotubes*; Imperial College Press: London, 1998.
- Tans, S. J.; Devoret, M. H.; Dai, H. J.; Thess, A.; Smalley, R. E.; Geerligs, L. J.; Dekker, C. Individual Single-Wall Carbon Nanotubes as Quantum Wires. *Nature* **1997**, *386*, 474–477.
- Wang, C.; Zhang, J.; Ryu, K.; Badmaev, A.; De Arco, L. G.; Zhou, C. Wafer-Scale Fabrication of Separated Carbon Nanotube Thin-Film Transistors for Display Applications. *Nano Lett.* **2009**, *9*, 4285–4291.
- Hong, S. W.; Banks, T.; Rogers, J. A. Improved Density in Aligned Arrays of Single-Walled Carbon Nanotubes by Sequential Chemical Vapor Deposition on Quartz. *Adv. Mater.* **2010**, *22*, 1826–1830.
- Wang, C. A.; Ryu, K. M.; De Arco, L. G.; Badmaev, A.; Zhang, J. L.; Lin, X.; Che, Y. C.; Zhou, C. W. Synthesis and Device Applications of High-Density Aligned Carbon Nanotubes Using Low-Pressure Chemical Vapor Deposition and Stacked Multiple Transfer. *Nano Res.* **2010**, *3*, 831–842.
- Zhou, W. W.; Ding, L.; Yang, S.; Liu, J. Synthesis of High-Density, Large-Diameter, and Aligned Single-Walled Carbon Nanotubes by Multiple-Cycle Growth Methods. *ACS Nano* **2011**, *5*, 3849–3857.
- Franklin, A. D.; Luisier, M.; Han, S. J.; Tulevski, G.; Breslin, C. M.; Gignac, L.; Lundstrom, M. S.; Haensch, W. Sub-10 nm Carbon Nanotube Transistor. *Nano Lett.* **2012**, *12*, 758–762.
- Park, H.; Afzali, A.; Han, S. J.; Tulevski, G. S.; Franklin, A. D.; Tersoff, J.; Hannon, J. B.; Haensch, W. High-Density Integration of Carbon Nanotubes via Chemical Self-Assembly. *Nat. Nanotechnol.* **2012**, *7*, 787–791.
- Kreupl, F. Electronics Carbon Nanotubes Finally Deliver. *Nature* **2012**, *484*, 321–322.
- Appenzeller, J. Carbon Nanotubes for High-Performance Electronics: Progress and Prospect. *Proc. IEEE* **2008**, *96*, 201–211.
- Avouris, P.; Martel, R. Progress in Carbon Nanotube Electronics and Photonics. *MRS Bull.* **2010**, *35*, 306–313.
- Franklin, A. D.; Chen, Z. H. Length Scaling of Carbon Nanotube Transistors. *Nat. Nanotechnol.* **2010**, *5*, 858–862.
- Patil, N.; Deng, J.; Mitra, S.; Wong, H. S. P. Circuit-Level Performance Benchmarking and Scalability Analysis of Carbon Nanotube Transistor Circuits. *IEEE Trans. Nanotechnol.* **2009**, *8*, 37–45.
- Kocabas, C.; Hur, S. H.; Gaur, A.; Meitl, M. A.; Shim, M.; Rogers, J. A. Guided Growth of Large-Scale, Horizontally Aligned Arrays of Single-Walled Carbon Nanotubes and Their Use in Thin-Film Transistors. *Small* **2005**, *1*, 1110–1116.
- Reina, A.; Hofmann, M.; Zhu, D.; Kong, J. Growth Mechanism of Long and Horizontally Aligned Carbon Nanotubes by Chemical Vapor Deposition. *J. Phys. Chem. C* **2007**, *111*, 7292–7297.
- Cao, Q.; Rogers, J. A. Ultrathin Films of Single-Walled Carbon Nanotubes for Electronics and Sensors: A Review of Fundamental and Applied Aspects. *Adv. Mater.* **2009**, *21*, 29–53.
- Che, Y. C.; Wang, C.; Liu, J.; Liu, B. L.; Lin, X.; Parker, J.; Beasley, C.; Wong, H. S. P.; Zhou, C. W. Selective Synthesis and Device Applications of Semiconducting Single-Walled Carbon Nanotubes Using Isopropyl Alcohol as Feedstock. *ACS Nano* **2012**, *6*, 7454–7462.
- Ding, L.; Tselev, A.; Wang, J. Y.; Yuan, D. N.; Chu, H. B.; McNicholas, T. P.; Li, Y.; Liu, J. Selective Growth of Well-Aligned Semiconducting Single-Walled Carbon Nanotubes. *Nano Lett.* **2009**, *9*, 800–805.
- Hong, G.; Zhang, B.; Peng, B.; Zhang, J.; Choi, W. M.; Choi, J. Y.; Kim, J. M.; Liu, Z. Direct Growth of Semiconducting Single-Walled Carbon Nanotube Array. *J. Am. Chem. Soc.* **2009**, *131*, 14642–14643.
- Li, P.; Zhang, J. Sorting out Semiconducting Single-Walled Carbon Nanotube Arrays by Preferential Destruction of Metallic Tubes Using Water. *J. Mater. Chem.* **2011**, *21*, 11815–11821.
- Li, W. S.; Hou, P. X.; Liu, C.; Sun, D. M.; Yuan, J. T.; Zhao, S. Y.; Yin, L. C.; Cong, H. T.; Cheng, H. M. High-Quality, Highly

- Concentrated Semiconducting Single-Wall Carbon Nanotubes for Use in Field Effect Transistors and Biosensors. *ACS Nano* **2013**, *7*, 6831–6839.
29. Li, Y. M.; Mann, D.; Rolandi, M.; Kim, W.; Ural, A.; Hung, S.; Javey, A.; Cao, J.; Wang, D. W.; Yenilmez, E.; *et al.* Preferential Growth of Semiconducting Single-Walled Carbon Nanotubes by a Plasma Enhanced CVD Method. *Nano Lett.* **2004**, *4*, 317–321.
  30. Parker, J.; Beasley, C.; Lin, A.; Chen, H. Y.; Wong, H. S. P. Increasing the Semiconducting Fraction in Ensembles of Single-Walled Carbon Nanotubes. *Carbon* **2012**, *50*, 5093–5098.
  31. Peng, B. H.; Jiang, S.; Zhang, Y. Y.; Zhang, J. Enrichment of Metallic Carbon Nanotubes by Electric Field-Assisted Chemical Vapor Deposition. *Carbon* **2011**, *49*, 2555–2560.
  32. Lu, C. G.; Liu, J. Controlling the Diameter of Carbon Nanotubes in Chemical Vapor Deposition Method by Carbon Feeding. *J. Phys. Chem. B* **2006**, *110*, 20254–20257.
  33. Zhou, W. W.; Zhan, S. T.; Ding, L.; Liu, J. General Rules for Selective Growth of Enriched Semiconducting Single Walled Carbon Nanotubes with Water Vapor as *In Situ* Etchant. *J. Am. Chem. Soc.* **2012**, *134*, 14019–14026.
  34. Yoshihara, N.; Ago, H.; Tsuji, M. Chemistry of Water-Assisted Carbon Nanotube Growth over Fe-Mo/Mgo Catalyst. *J. Phys. Chem. C* **2007**, *111*, 11577–11582.
  35. Lu, J.; Nagase, S.; Zhang, X. W.; Wang, D.; Ni, M.; Maeda, Y.; Wakahara, T.; Nakahodo, T.; Tsuchiya, T.; Akasaka, T.; *et al.* Selective Interaction of Large or Charge-Transfer Aromatic Molecules with Metallic Single-Wall Carbon Nanotubes: Critical Role of the Molecular Size and Orientation. *J. Am. Chem. Soc.* **2006**, *128*, 5114–5118.
  36. Ding, L.; Yuan, D. N.; Liu, J. Growth of High-Density Parallel Arrays of Long Single-Walled Carbon Nanotubes on Quartz Substrates. *J. Am. Chem. Soc.* **2008**, *130*, 5428–5429.
  37. Zhou, W. W.; Rutherglen, C.; Burke, P. J. Wafer Scale Synthesis of Dense Aligned Arrays of Single-Walled Carbon Nanotubes. *Nano Res.* **2008**, *1*, 158–165.
  38. Amama, P. B.; Pint, C. L.; McJilton, L.; Kim, S. M.; Stach, E. A.; Murray, P. T.; Hauge, R. H.; Maruyama, B. Role of Water in Super Growth of Single-Walled Carbon Nanotube Carpets. *Nano Lett.* **2009**, *9*, 44–49.
  39. Hasegawa, K.; Noda, S. Moderating Carbon Supply and Suppressing Ostwald Ripening of Catalyst Particles To Produce 4.5-mm-Tall Single-Walled Carbon Nanotube Forests. *Carbon* **2011**, *49*, 4497–4504.
  40. Dresselhaus, M. S.; Dresselhaus, G.; Saito, R.; Jorio, A. Raman Spectroscopy of Carbon Nanotubes. *Phys. Rep.* **2005**, *409*, 47–99.
  41. Liu, K. H.; Hong, X. P.; Zhou, Q.; Jin, C. H.; Li, J. H.; Zhou, W. W.; Liu, J.; Wang, E. G.; Zettl, A.; Wang, F. High-Throughput Imaging and Spectroscopy of Individual Carbon Nanotubes in Devices with Light Microscopy. *Nat. Nanotechnol.* **2013**, DOI: 10.1038/nnano.2013.227.
  42. Zhang, G. Y.; Qi, P. F.; Wang, X. R.; Lu, Y. R.; Li, X. L.; Tu, R.; Bangsaruntip, S.; Mann, D.; Zhang, L.; Dai, H. J. Selective Etching of Metallic Carbon Nanotubes by Gas-Phase Reaction. *Science* **2006**, *314*, 974–977.
  43. Srivastava, D.; Brenner, D. W.; Schall, J. D.; Ausman, K. D.; Yu, M. F.; Ruoff, R. S. Predictions of Enhanced Chemical Reactivity at Regions of Local Conformational Strain on Carbon Nanotubes: Kinky Chemistry. *J. Phys. Chem. B* **1999**, *103*, 4330–4337.
  44. Astakhova, T. Y.; Vinogradov, G. A.; Gurin, O. D.; Menon, M. Effect of Local Strain on the Reactivity of Carbon Nanotubes. *Russ. Chem. Bull.* **2002**, *51*, 764–769.